DEUTSCHES ELEKTRONEN-SYNCHROTRON DESY

DESY 68/48
September 1968

Inelastic Electron Proton Scattering at High Momentum Transfers

W. Albrecht, F. W. Brasse, H. Dorner, W. Flauger, K. Frank, J. Gayler, H. Hultschig, and J. May

Deutsches Elektronen-Synchrotron DESY, Hamburg

and

E. Ganßauge

Universität Marburg

2 HAMBURG 52 · NOTKESTIEG 1

INELASTIC ELECTRON PROTON SCATTERING AT HIGH MOMENTUM TRANSFERS

by

W. Albrecht, F.W. Brasse, H. Dorner, W. Flauger, K. Frank
J. Gayler, H. Hultschig, and J. May, DESY Hamburg

and

E. Ganßauge, Universität Marburg

ABSTRACT

Inelastic electron proton scattering has been measured by detecting the scattered electron, thus obtaining the total absorption cross section for virtual photons. Two complete spectra from threshold to a pion nucleon mass of W = 2 GeV were taken at $\vartheta_e = 48.3^\circ$ and fixed primary energies of 3.963 GeV and 5.159 GeV, respectively, corresponding to a momentum transfer at the first resonance of $q^2 = 3.98\ (\mathrm{GeV/c})^2$ and $q^2 = 5.84\ (\mathrm{GeV/c})^2$. In addition, a measurement at $\vartheta_e = 47.9^\circ$ and at a primary energy of 3.306 GeV in the region of the first resonance is reported.

The apparatus used for these measurements was essentially the same as that one, which had been used already for elastic electron proton scattering [1] and for a part of the first inelastic measurements [2]. A liquid hydrogen target is located inside the vacuum pipe of the synchrotron. It is hit by the internal electron beam at the end of each acceleration cycle by use of the beam bump method. A magnetic spectrometer can swing around the target within a limited range of angle. It consists of two quadrupoles for focussing in both planes and of a magnet, which bends the particles in the horizontal plane. A set of scintillation counters defines 7 momentum channels with a total acceptance of 2.8%. Electrons are identified by a Čerenkov and a shower counter.

A quantameter was used as a relative monitor for the intensity of the primary beam. The absolute calibration however was achieved as in former measurements [1] by detecting recoil protons from elastic scattering at a momentum transfer of 0.51 $(GeV/c)^2$, where the form factors of the proton are well known.

The contribution to the counting rate, coming from the target walls (a cylinder of 11 mm diameter made out of 12μ polyimid foil) was measured by replacing the full target by a piece of the foil material presenting the same number of radiation lengths to the primary electrons as the full target. In the case of the full target a certain fraction δ_f of the bremsstrahlung going into the quantameter comes from the target wall. This fraction δ_f was determined from the proton recoil measurements. For subtracting the counting rate of the target wall the same fraction δ_f of the measured rate per quantameter charge was used. δ_f was around 25% and the counting rate, which had to be subtracted, was at its highest value 15% of the full target rate.

For fixed primary energy and fixed scattering angle the inelastic spectrum was taken from threshold to W = 2 GeV in steps of 2.8% of the momentum of the secondary electron. At certain intervals the rate of positrons was determined in order to subtract electrons coming from π^o decay. At its highes value this rate was 7% of the total electron rate. Also for the target wall measurements this rate has been determined.

The cross sections had to be corrected further for radiation processes. The wide angle bremsstrahlung (WAB) was calculated by the peaking method as well as by the more correct method described by Mo and Tsai [3]. In the experimental range of energies both methods gave the same result within 2 % of the uncorrected cross section. The radiation of the electron during inelastic scattering was also calculated by the peaking method. For the interpolation of inelastic cross sections needed to perform the calculations two different methods were used. One was the $|\vec{q}|^b$ dependence with b = b (W) as found in the earlier measurements [2]. For the other method individual empirical fits to the cross sections for different values of W and as functions of the four-momentum transfer q^2 were used. However, both methods agreed within 2% of the cross section. Finally, the Schwinger effect was calculated by a formula of Yennie, Frautschi and Suura [4].

There is a drastic change of the complete radiative correction at high masses W going from low to high momentum transfers. At low momentum transfers ($q^2_{2000} = 0.47$ (GeV/c)^2) the total radiative correction for W = 2 GeV is 30% of the uncorrected value, whereas at the momentum transfer $q^2_{2000} = 4.24$ (GeV/c)^2 the total correction is only 1.1%. This is due to the fact, that the cross section for low masses (especially for the proton

itself and the first resonance) falls off more rapidly with increasing momentum transfer than the one for high masses.

The corrected cross sections for the three spectra are shown in the form

$$\sum_t = \frac{1}{\Gamma_t} \frac{d^2\sigma}{d\Omega dE'} = \sigma_t + \varepsilon\sigma_l$$

as a function of the pion nucleon mass W in Figs. 1 - 3. One can see that the 1236-resonance is vanishing remarkably with increasing momentum transfer within the nonresonant background. At $q^2 = 5.84\ (GeV/c)^2$ the resonance is already difficult to be recognized. But also the bumps at the higher resonances, comparing them with those at lower momentum transfers [2], almost vanish within the background and the statistical errors.

In Tables 1 - 3 the cross sections and the corresponding kinematic data are listed. The first value above the threshold contains a large systematic error in the radiative correction because of the rather large steps in W. Table 4 gives the cross section for some specific resonant and non-resonant values of W.

In Fig. 4 the cross section $\sum_t$, divided by the square of the normalized magnetic form factor of the proton, is plotted against the square of the three-momentum transfer $|\vec{q}|$ in a double logarithmic scale for the 1236-resonance. The figure contains also the results from other laboratories [6)7)] as well as the results of Brasse et al. [2)]. In the case of the data of Lynch et al. [6)] only the transverse part σ_t is shown. In the range of $0.78 \leq q^2 \leq 2.31\ (GeV/c)^2$ it is shown by Bartel et al. [8)], if they combine their data with those from Brasse et al. [2)], that σ_l is practically zero. It is assumed

therefore for the measurements at higher momentum transfers, where in Fig. 4 $\sum_t$ is plotted instead of σ_t, that $\varepsilon\sigma_l$ is small compared to σ_t. For our new data the proton form factor was taken from the dipole fit, whereas for the data at lower momentum transfers short range fits to the measured form factors were used. The figure also shows the dispersion theoretic calculation of Gutbrod and Simon [9]. At $q^2 = 0$ their calculation is normalized to the result of the static theory, which is higher than the total photoproduction cross section, obtained by integration of the measured differential photoproduction cross sections [10]. In their calculations the pion form factor was set equal to the nucleon form factor. The agreement with the measurements is remarkably good. Up to a three-momentum transfer of about 3 $(GeV/c)^2$ the cross section is well represented by a straight line as indicated in figure 4. At high momentum transfer the measured cross section does no longer follow the straight line behaviour, but falls off to lower values, even lower than the dispersion theoretic calculation. Since the data represent resonant and nonresonant part together and since one sees from the spectra that the resonant contribution is vanishing with increasing momentum transfer, one may conclude, that the γNN^* form factor is decreasing faster than the nucleon form factor in this range of momentum transfer. This is shown also by recent measurements from Bartel et al. [11].

Also for higher masses W the cross section as plotted in figure 1 (Fig. 5 and 6) does no longer follow the straight line behaviour, which was found for the measurements at lower momentum transfers [2].

The data are summarized in Fig. 7, where $\sum_t$ is plotted against the four-momentum transfer in a half logarithmic scale. The curves are fitted parabolas in this representation. The photoproduction values [10)12)] have not been taken into account for the fits, since the straight line behaviour in the $|\vec{q}|^2$

representation (which corresponds to a threshold behaviour) requires at very small momentum transfer a curve different from the one used for the fit. Fig. 7 shows that for a fixed small momentum transfer the cross section decreases with increasing mass W of the final state. At large momentum transfers, however, the cross section first increases with W and then stays constant.

We are indebted to Professor W. Jentschke and Professor M. Teucher for their support of this experiment, and to the entire machine staff of DESY for the excellent performance of the synchrotron.

Figure captions:

Fig. 1 - 3 : The measured absorption cross section for virtual photons as function of the mass W of the pion nucleon system.

Fig. 4 : The measured absorption cross section for virtual photons, divided by the square of the normalized magnetic proton form factor, compared with the dispersion theoretic calculation [9] as function of the square of the three-momentum transfer $|\vec{q}|$.

Fig. 5 and 6 : The measured absorption cross section for virtual photons as function of the square of the three-momentum transfer $|\vec{q}|$ for W = 1.525 and 1.688 GeV.

Fig. 7 : The measured absorption cross section for virtual photons for different masses W as function of the square of the four-momentum transfer. The curves are fitted parabolas.

REFERENCES:

1) W. Albrecht, H.-J. Behrend, F.W. Brasse, W. Flauger, H. Hultschig and K.G. Steffen, Phys. Rev. Let. 17, 1192 (1966).

2) F. W. Brasse, J. Engler, E. Ganßauge and M. Schweizer, Nuov. Cim. 55A, 679 (1968), also DESY 67/34 (1967).

3) L.W. Mo and Y.S. Tsai SLAC-PUB-380 (1968).

4) D.R. Yennie, S.C. Frautschi and H. Suura, Ann. Phys. 13, 379 (1961)

5) The same notation is used as in reference 2).

6) H.L. Lynch, J.V. Allaby and D.M. Ritson, HEPL-494 B (1967).

7) A.A. Cone, K.W. Chen, J.R. Dunning, G. Hartwig, N.F. Ramsey, J.K. Walker, R. Wilson, Phys. Rev. 156, 1490 (1967).

8) W. Bartel, B. Dudelzak, H. Krehbiel, J. McElroy, U. Meyer-Berkhout, W. Schmidt, V. Walther and G. Weber, DESY 68/42 (1968), also Phys. Let. 27B, 660 (1968).

9) F. Gutbrod and D. Simon, Nuov. Cim. 51A, 602 (1967).

10) Data Compilation by J.T. Beale, S.D. Ecklund, R.L. Walker, Report CTSL-42, CALT-68-108.

11) W. Bartel, B. Dudelzak, H. Krehbiel, J. McElroy, U. Meyer-Berkhout, W. Schmidt, V. Walther and G. Weber,
DESY 68/53 (1968), also to be published.

12) DESY Bubble Chamber Collaboration
DESY 68/31 (1968).

TABLE 1

Kinematic values and cross sections for the measurement E_o = 3.306 GeV, ϑ = 47.89°. Cross sections are averaged over 3.5 adjacent momentum channels.

E'	W	q^2	Γ_t	$d^2\sigma/d\Omega dE'$	stat. error	rad. correction	$\frac{1}{\Gamma_t} d^2\sigma/d\Omega dE'$
[GeV]	[GeV]	$[(GeV/c)^2]$	$[GeV^{-1}ster^{-1}]$	$[cm^2/GeVster]$	[%]	$[cm^2/GeVster]$	$[cm^2]$
1.469	1.062	3.200	1.515E-05	3.42E-36	26.0	9.12E-35	2.25E-31
1.448	1.101	3.155	2.005E-05	1.14E-34	19.5	5.41E-35	5.71E-30
1.428	1.137	3.112	2.465E-05	1.47E-34	20.8	3.47E-36	5.98E-30
1.408	1.172	3.068	2.922E-05	2.95E-34	11.0	-2.52E-35	1.01E-29
1.389	1.205	3.026	3.351E-05	5.11E-34	8.4	-4.56E-35	1.52E-29
1.370	1.237	2.983	3.777E-05	6.03E-34	6.3	-5.11E-35	1.60E-29
1.351	1.267	2.943	4.176E-05	6.39E-34	6.1	-4.23E-35	1.53E-29
1.332	1.297	2.901	4.573E-05	6.56E-34	7.3	-2.70E-35	1.43E-29
1.314	1.325	2.862	4.945E-05	6.67E-34	7.2	-1.42E-35	1.35E-29
1.295	1.353	2.822	5.315E-05	6.88E-34	10.1	-7.08E-36	1.30E-29
1.278	1.380	2.783	5.662E-05	7.26E-34	9.9	-4.91E-36	1.28E-29
1.260	1.406	2.744	6.007E-05	8.78E-34	9.0	-6.61E-36	1.46E-29
1.243	1.430	2.707	6.330E-05	8.15E-34	9.5	-1.68E-35	1.29E-29
1.225	1.455	2.669	6.652E-05	1.08E-33	8.4	-3.57E-35	1.62E-29
1.208	1.478	2.632	6.953E-05	1.25E-33	7.9	-5.12E-35	1.80E-29

TABLE 2

Kinematic values and cross sections for the measurement E_o = 3.963 GeV, ϑ = 48.29°. Cross sections are averaged over 3.5 adjacent momentum channels.

E'	W	q^2	Γ_t	$d^2\sigma/d\Omega dE'$	stat. error	rad. correction	$\frac{1}{\Gamma_t} d^2\sigma/d\Omega dE'$
[GeV]	[GeV]	$[(GeV/c)^2]$	$[GeV^{-1}ster^{-1}]$	$[cm^2/GeVster]$	[%]	$[cm^2/GeVster]$	$[cm^2]$
1.586	1.065	4.207	9.808E-06	7.11E-36	19.4	3.92E-35	7.25E-31
1.564	1.111	4.148	1.357E-05	1.27E-35	17.1	2.24E-35	9.38E-31
1.542	1.154	4.091	1.711E-05	4.88E-35	14.6	-3.16E-36	2.85E-30
1.521	1.196	4.034	2.063E-05	1.17E-34	9.3	-1.11E-35	5.68E-30
1.500	1.234	3.978	2.394E-05	1.52E-34	8.0	-1.39E-35	6.36E-30
1.479	1.272	3.923	2.724E-05	1.79E-34	9.2	-1.35E-35	6.56E-30
1.459	1.308	3.869	3.033E-05	1.92E-34	8.7	-1.05E-35	6.34E-30
1.438	1.343	3.815	3.341E-05	2.09E-34	9.2	-5.61E-36	6.25E-30
1.419	1.376	3.763	3.631E-05	1.75E-34	10.3	-2.74E-36	4.81E-30
1.399	1.408	3.710	3.919E-05	2.63E-34	8.1	-4.98E-36	6.71E-30
1.380	1.438	3.659	4.191E-05	2.55E-34	8.5	-1.50E-35	6.08E-30
1.360	1.469	3.608	4.460E-05	3.85E-34	8.5	-3.24E-35	8.62E-30
1.342	1.497	3.559	4.714E-05	5.06E-34	7.3	-4.88E-35	1.07E-29
1.323	1.525	3.509	4.967E-05	6.40E-34	8.7	-5.56E-35	1.29E-29
1.305	1.552	3.461	5.205E-05	6.82E-34	8.3	-4.73E-35	1.31E-29
1.286	1.578	3.412	5.441E-05	6.06E-34	9.0	-2.81E-35	1.11E-29
1.269	1.603	3.366	5.664E-05	7.09E-34	8.1	-8.56E-36	1.25E-29
1.251	1.628	3.318	5.886E-05	5.74E-34	9.3	2.85E-36	9.75E-30
1.234	1.652	3.273	6.095E-05	6.69E-34	8.6	-2.42E-36	1.10E-29
1.217	1.675	3.227	6.303E-05	8.17E-34	7.9	-2.23E-35	1.30E-29
1.200	1.698	3.183	6.499E-05	8.79E-34	7.7	-4.00E-35	1.35E-29
1.183	1.720	3.138	6.694E-05	1.20E-33	6.5	-3.98E-35	1.79E-29
1.167	1.741	3.095	6.878E-05	1.07E-33	6.9	-2.58E-35	1.55E-29
1.151	1.762	3.052	7.061E-05	1.04E-33	8.4	-1.72E-35	1.47E-29
1.135	1.782	3.010	7.233E-05	1.17E-33	7.9	-2.14E-35	1.62E-29
1.119	1.803	2.968	7.405E-05	1.52E-33	6.8	-1.66E-35	2.05E-29
1.104	1.822	2.928	7.567E-05	1.30E-33	7.5	5.28E-36	1.71E-29
1.088	1.841	2.886	7.728E-05	1.20E-33	7.9	2.74E-35	1.55E-29
1.073	1.859	2.847	7.881E-05	1.35E-33	7.4	2.88E-35	1.71E-29
1.058	1.877	2.807	8.032E-05	1.60E-33	6.8	1.94E-35	1.99E-29
1.044	1.895	2.769	8.176E-05	1.61E-33	6.9	1.91E-35	1.97E-29
1.029	1.912	2.730	8.318E-05	1.64E-33	6.9	3.14E-35	1.97E-29
1.015	1.929	2.693	8.453E-05	1.64E-33	6.9	4.33E-35	1.94E-29
1.001	1.945	2.655	8.587E-05	1.92E-33	6.4	5.30E-35	2.24E-29
0.987	1.961	2.619	8.714E-05	1.75E-33	6.8	6.76E-35	2.01E-29
0.973	1.977	2.582	8.841E-05	1.98E-33	6.4	9.35E-35	2.24E-29
0.960	1.992	2.547	8.960E-05	1.80E-33	6.7	1.18E-34	2.01E-29
0.947	2.007	2.511	9.079E-05	1.95E-33	6.5	1.23E-34	2.14E-29
0.934	2.022	2.476	9.192E-05	2.17E-33	6.2	9.42E-35	2.36E-29

TABLE 3

Kinematic values and cross sections for the measurement E_o = 5.159 GeV, ϑ = 48.12°. Cross sections are averaged over 3.5 adjacent momentum channels.

E'	W	q^2	Γ_t	$d^2\sigma/d\Omega dE'$	stat. error	rad. correction	$\frac{1}{\Gamma_t} d^2\sigma/d\Omega dE'$
[GeV]	[GeV]	$[(GeV/c)^2]$	$[GeV^{-1}ster^{-1}]$	$[cm^2/GeVster]$	[%]	$[cm^2/GeVster]$	$[cm^2]$
1.786	1.040	6.127	4.221E-06	7.97E-36	28.0	3.16E-36	1.89E-30
1.762	1.101	6.043	6.868E-06	-1.85E-36	101.7	4.06E-36	-2.69E-31
1.737	1.159	5.959	9.506E-06	1.80E-35	16.1	8.09E-38	1.89E-30
1.713	1.212	5.877	1.199E-05	2.66E-35	13.2	-2.20E-36	2.22E-30
1.689	1.263	5.795	1.447E-05	2.30E-35	17.5	-2.87E-36	1.59E-30
1.666	1.311	5.716	1.681E-05	3.67E-35	12.3	-3.07E-36	2.18E-30
1.643	1.358	5.635	1.913E-05	5.13E-35	14.3	-3.21E-36	2.68E-30
1.621	1.401	5.558	2.133E-05	5.39E-35	14.2	-4.56E-36	2.53E-30
1.598	1.443	5.480	2.352E-05	6.35E-35	16.8	-8.22E-36	2.70E-30
1.576	1.483	5.405	2.558E-05	9.26E-35	13.2	-1.18E-35	3.62E-30
1.554	1.522	5.330	2.764E-05	1.52E-34	15.2	-1.10E-35	5.49E-30
1.533	1.558	5.257	2.958E-05	1.11E-34	19.3	-5.57E-36	3.76E-30
1.511	1.595	5.183	3.152E-05	1.06E-34	18.8	-7.14E-37	3.35E-30
1.490	1.629	5.112	3.335E-05	9.12E-35	21.3	-3.63E-36	2.74E-30
1.470	1.662	5.041	3.517E-05	1.86E-34	15.5	-1.41E-35	5.30E-30
1.449	1.694	4.972	3.689E-05	2.19E-34	14.5	-2.48E-35	5.95E-30
1.429	1.726	4.902	3.861E-05	3.02E-34	15.4	-2.79E-35	7.83E-30
1.410	1.755	4.835	4.023E-05	3.02E-34	15.3	-2.22E-35	7.52E-30
1.390	1.785	4.767	4.185E-05	3.02E-34	15.5	-1.05E-35	7.23E-30
1.371	1.813	4.702	4.338E-05	2.29E-34	18.3	-3.58E-36	5.28E-30
1.352	1.841	4.636	4.490E-05	3.20E-34	15.2	-2.73E-36	7.13E-30
1.333	1.867	4.573	4.634E-05	3.04E-34	15.9	-6.18E-36	6.55E-30
1.314	1.894	4.509	4.778E-05	3.65E-34	14.6	-9.48E-36	7.64E-30
1.296	1.919	4.447	4.915E-05	3.53E-34	15.1	-1.04E-35	7.18E-30
1.278	1.944	4.385	5.051E-05	4.49E-34	13.2	-8.69E-36	8.89E-30
1.261	1.967	4.325	5.179E-05	4.29E-34	13.7	-6.18E-36	8.29E-30
1.243	1.991	4.264	5.307E-05	3.69E-34	12.5	-4.42E-36	6.95E-30
1.226	2.014	4.206	5.429E-05	4.82E-34	10.7	-3.15E-36	8.88E-30

Table 4: Total cross sections of electro-production for various values of the mass W of the outgoing nucleon system

W [GeV]	ϑ [°]	E_o [GeV]	E' [GeV]	q^2 [f^{-2}]	q^2 [$(GeV/c)^2$]	ε	Γ_t [$GeV^{-1} \cdot 10^5$]	$\lvert\vec{q}\rvert^2$ [$(GeV/c)^2$]	$\frac{1}{\Gamma_t} \cdot \frac{d^2\sigma}{d\Omega dE'}$ [$10^{-29}\,cm^2$]	stat. error [%]
1236	47.9	3.306	1.371	76.7	2.99	0.529	3.76	6.73	1.594	6.3
	48.3	3.963	1.499	102.1	3.98	0.496	2.41	10.05	0.637	8.0
	48.1	5.159	1.702	150.0	5.84	0.452	1.32	17.79	0.190	13.0
1470	47.9	3.306	1.214	67.9	2.64	0.489	6.85	7.02	1.741	9.0
	48.3	3.963	1.359	92.6	3.61	0.463	4.47	10.38	0.874	8.5
	48.1	5.159	1.583	139.5	5.43	0.428	2.49	18.22	0.334	13.2
1525	48.3	3.963	1.323	90.1	3.51	0.455	4.97	10.48	1.287	8.7
	48.1	5.159	1.552	136.7	5.32	0.421	2.78	18.33	0.533	15.2
1615	48.3	3.963	1.260	85.8	3.34	0.438	5.77	10.65	1.000	8.6
	48.1	5.159	1.499	132.1	5.15	0.409	3.25	18.54	0.310	18.8
1688	48.3	3.963	1.207	82.2	3.20	0.425	6.41	10.80	1.328	7.8
	48.1	5.159	1.453	128.0	4.98	0.400	3.66	18.72	0.583	15.5
1820	48.3	3.963	1.104	75.2	2.93	0.396	7.57	11.10	1.714	7.5
	48.1	5.159	1.365	120.4	4.69	0.381	4.38	19.07	0.665	15.2
1920	48.3	3.963	1.022	69.7	2.71	0.373	8.38	11.36	1.957	6.9
	48.1	5.159	1.296	114.1	4.45	0.365	4.92	19.37	0.727	15.1

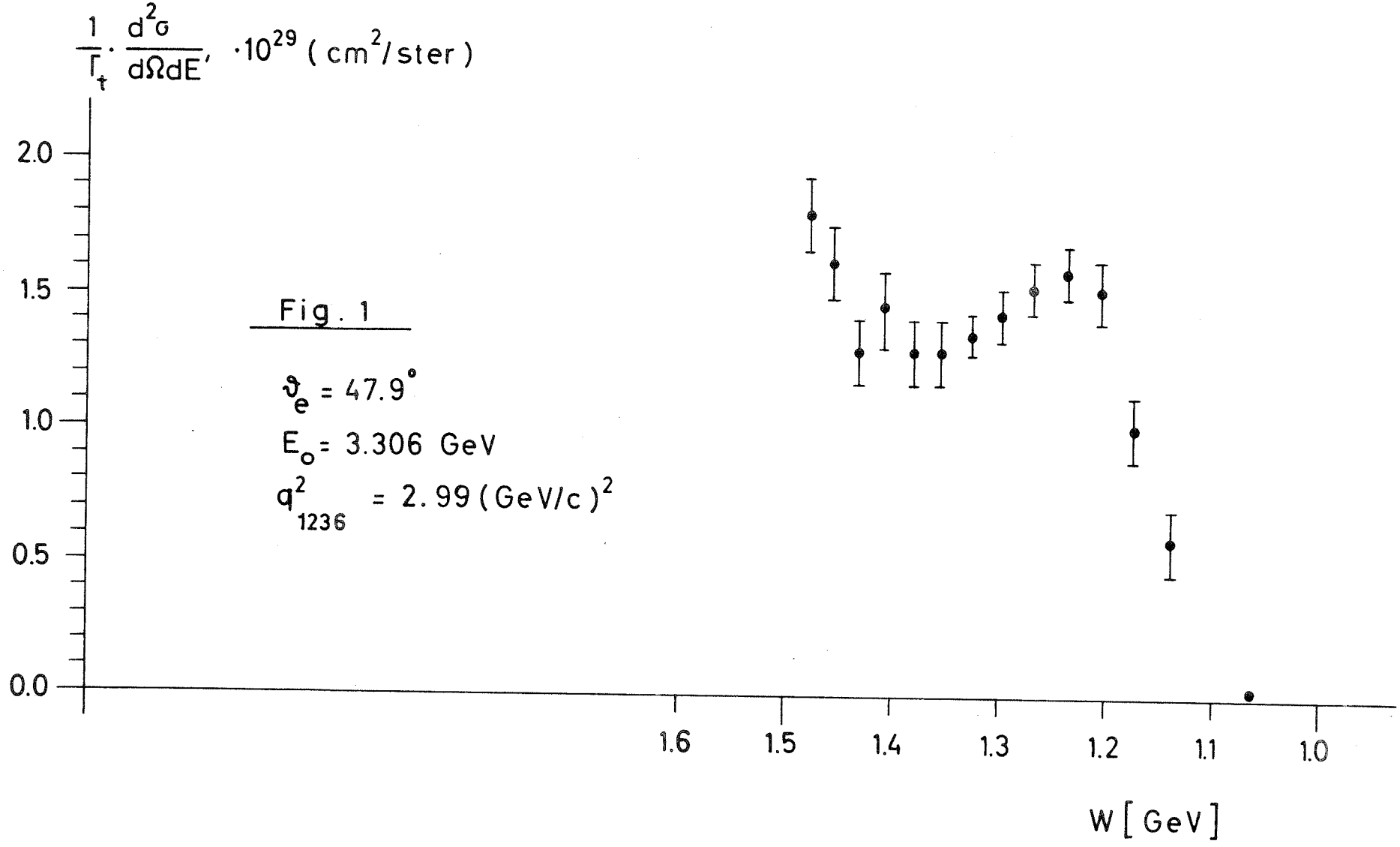

Fig. 1

$\vartheta_e = 47.9°$

$E_o = 3.306$ GeV

$q^2_{1236} = 2.99\,(\mathrm{GeV/c})^2$

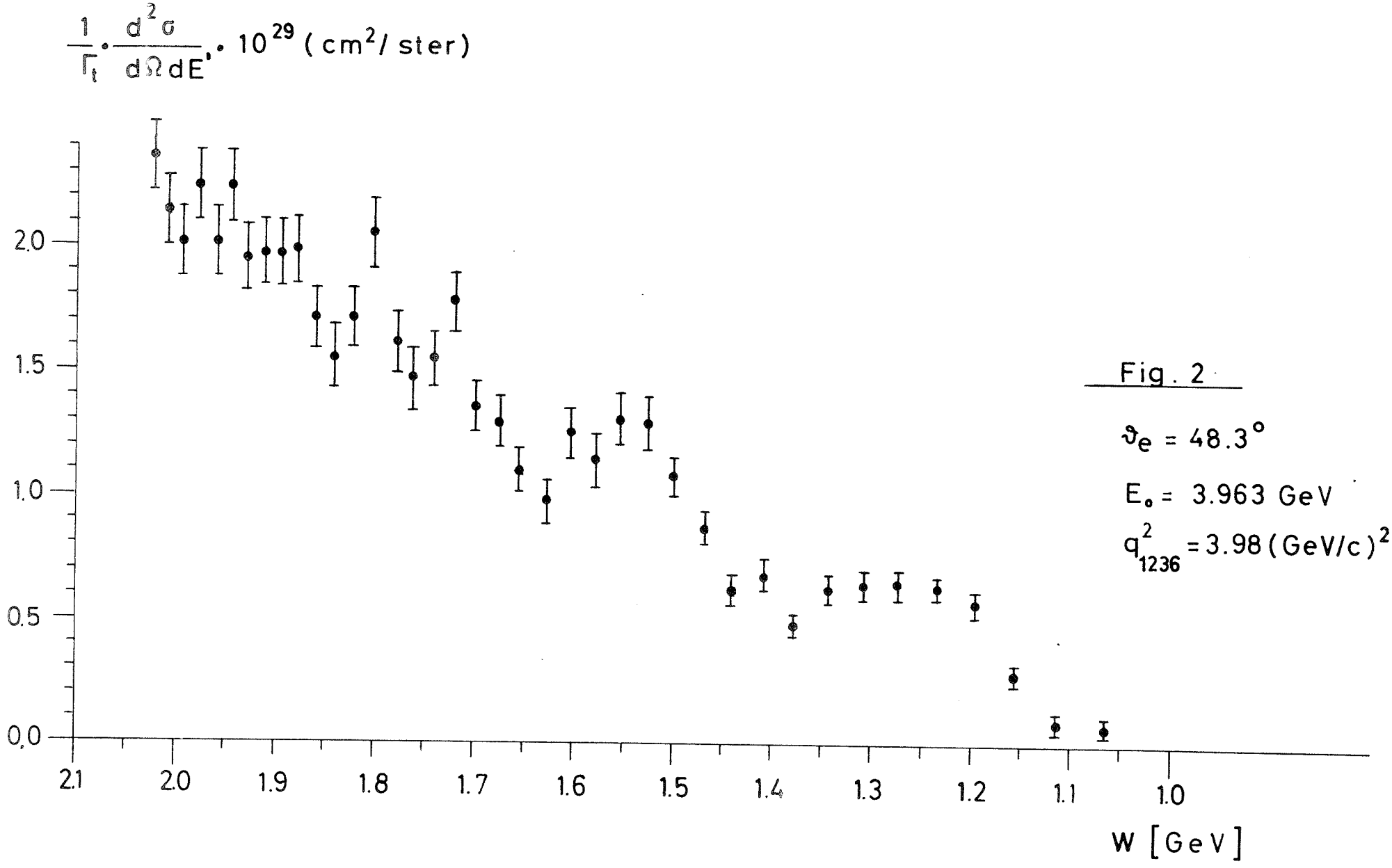

Fig. 2

$\vartheta_e = 48.3°$

$E_o = 3.963$ GeV

$q^2_{1236} = 3.98\,(GeV/c)^2$

$$\frac{1}{\Gamma_t} \cdot \frac{d^2\sigma}{d\Omega dE'} \cdot 10^{29} \; (cm^2/ster)$$

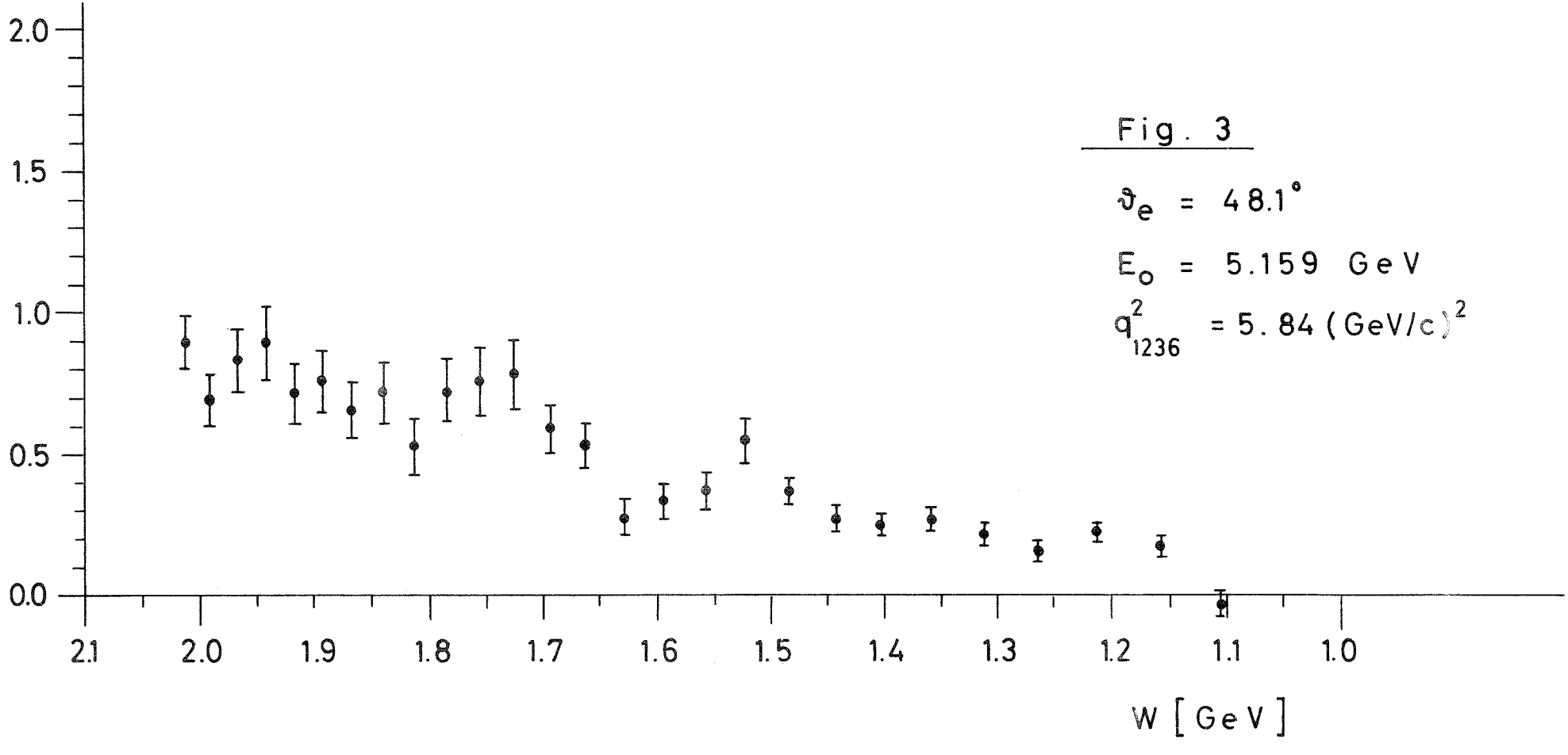

Fig. 3

$\vartheta_e = 48.1°$

$E_o = 5.159$ GeV

$q^2_{1236} = 5.84 \; (GeV/c)^2$

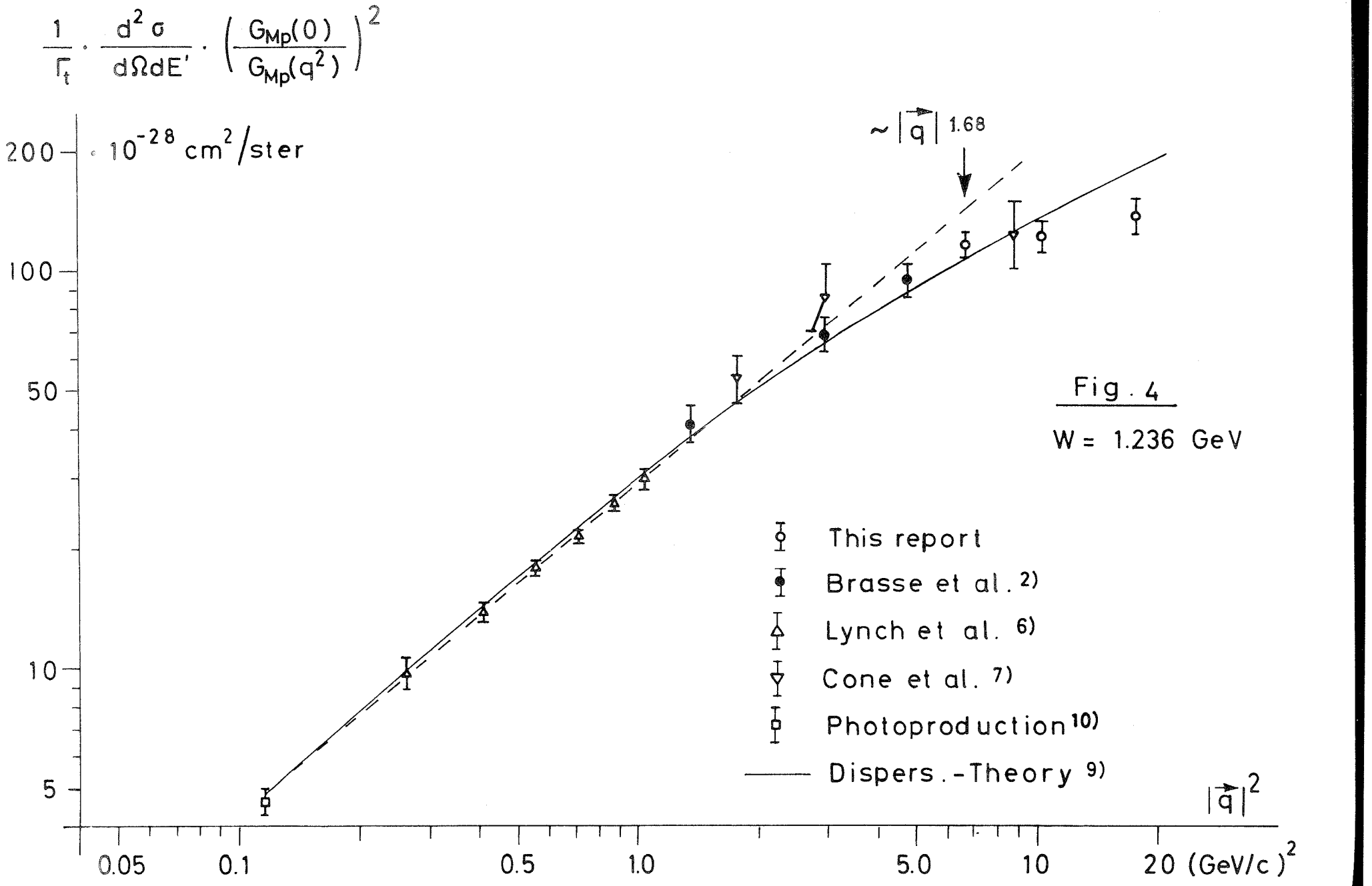
$\frac{1}{\Gamma_t} \cdot \frac{d^2\sigma}{d\Omega dE'} \cdot \left(\frac{G_{Mp}(0)}{G_{Mp}(q^2)}\right)^2$
$\cdot 10^{-28}$ cm^2/ster
200
100
50
10
5
$\sim |\vec{q}|$ 1.68
Fig. 4
W = 1.236 GeV
This report
Brasse et al. 2)
Lynch et al. 6)
Cone et al. 7)
Photoproduction 10)
Dispers.-Theory 9)
$|\vec{q}|^2$
0.05
0.1
0.5
1.0
5.0
10
20 (GeV/c)^2

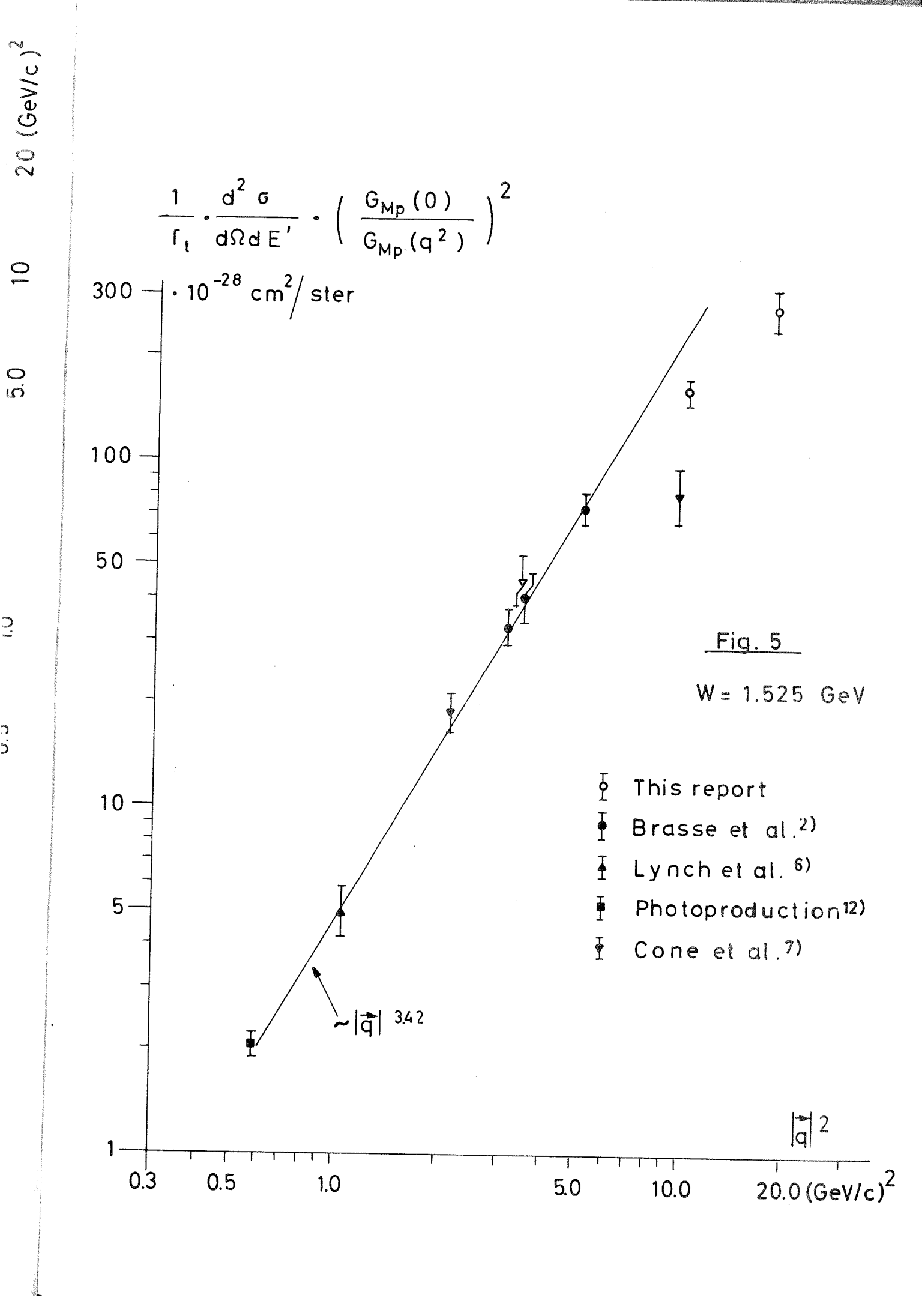
$\frac{1}{\Gamma_t} \cdot \frac{d^2\sigma}{d\Omega dE'} \cdot \left(\frac{G_{Mp}(0)}{G_{Mp}(q^2)} \right)^2$
$\cdot 10^{-28}$ cm^2/ ster
300
100
50
10
5
1
0.3
0.5
1.0
5.0
10.0
20.0 (GeV/c)^2
$|\vec{q}|^2$
$\sim |\vec{q}|^{3.42}$
This report
Brasse et al.[2)]
Lynch et al.[6)]
Photoproduction[12)]
Cone et al.[7)]
W = 1.525 GeV

Fig. 5

$$\frac{1}{\Gamma_t} \cdot \frac{d^2\sigma}{d\Omega dE'} \cdot \left(\frac{G_{Mp}(0)}{G_{Mp}(q^2)}\right)^2$$

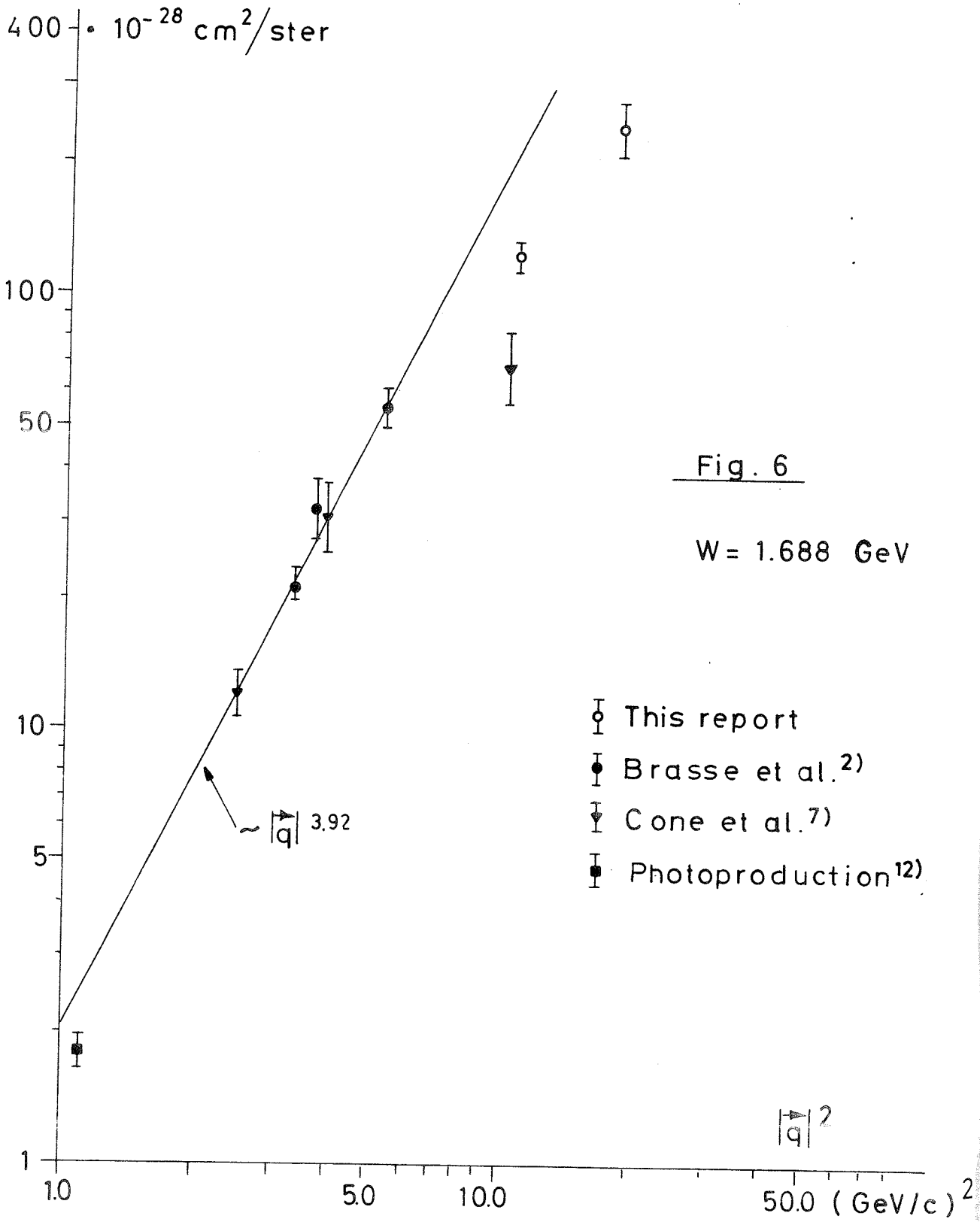

Fig. 6

W = 1.688 GeV

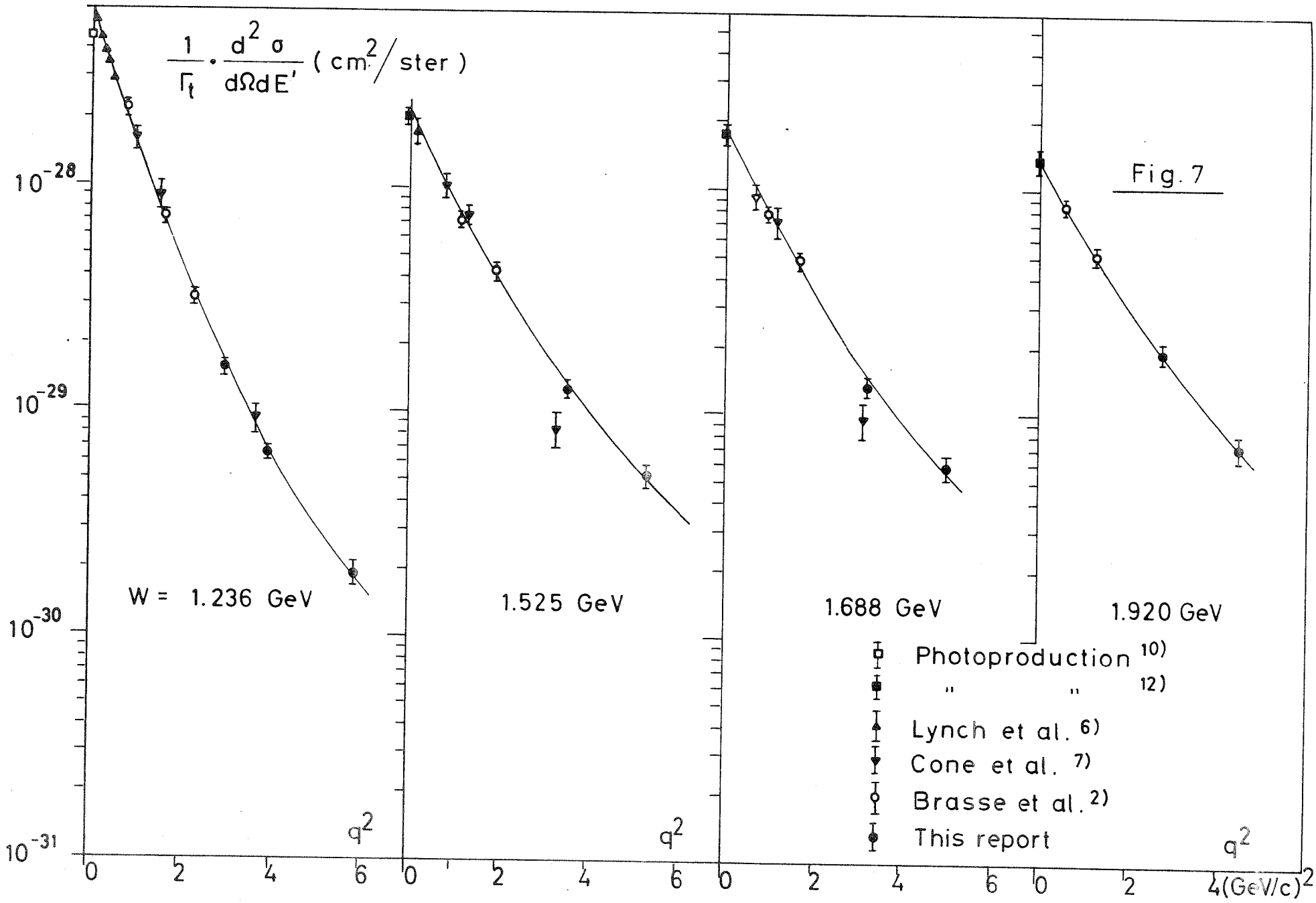
$\frac{1}{\Gamma_t} \cdot \frac{d^2\sigma}{d\Omega dE'}$ (cm^2/ster)
10^{-28}
10^{-29}
10^{-30}
10^{-31}
W = 1.236 GeV
1.525 GeV
1.688 GeV
1.920 GeV
q^2
0
2
4
6
$(GeV/c)^2$
Photoproduction 10)
" " 12)
Lynch et al. 6)
Cone et al. 7)
Brasse et al. 2)
This report

Fig. 7